Diffusion properties of gradient-based lattice Boltzmann models of immiscible fluids

M. Latva-Kokko and Daniel H. Rothman
Department of Earth Atmospheric and Planetary Sciences, Massachusetts Institute of Technology, 77 Massachusetts Avenue, Cambridge, Massachusetts 02139-4307, USA
(Received 3 December 2004; published 12 May 2005)

We study the diffusion and phase separation properties of a gradient- based lattice Boltzmann model of immiscible fluids. We quantify problems of lattice pinning associated with the model, and suggest a scheme that removes these artifacts. The interface width is controlled by a single parameter that acts as an inverse diffusion length. We derive an analytic expression of a fully developed interfacial curve and show that interfaces evolve towards this stable distribution if no fluid is trapped. Fluid can become trapped inside a competing phase if no connecting path to the bulk phase exists. Such trapped bubbles also evolve towards the fully developed interfacial curve but constraints on mass conservation limit this development. We also show how small numerical errors lead to spontaneous phase separation for all values of the diffusion length.

DOI: 10.1103/PhysRevE.71.056702 PACS number(s): 47.11.+j, 47.55.Kf, 05.10.−a

I. INTRODUCTION

Since the development of the lattice Boltzmann (LB) method [1–3] it has often been used to study complex multiphase fluid flow [4–8]. The fundamental idea of the LB method is to construct simplified kinetic models that incorporate the essential physics of microscopic or mesoscopic processes. Macroscopic or hydrodynamic behaviors such as interface dynamics naturally emerge as a result of these kinetics provided that correct conservation laws and symmetries such as rotational invariance are followed. The macroscopic dynamics of the fluid is the result of the collective behavior of many microscopic particles and is not sensitive to the underlying microscopic physics.

There are several LB models for simulation of immiscible multiphase flow. Here we study the method based on color gradients [9]. The color-gradient method retains sharp interfaces and the surface tension in this model is set by a single adjustable parameter and may be calculated analytically [5,9]. An alternative multiphase LB model proposed by Shan and Chen [10] is based on microscopic interactions between particles. This model also has sharp interfaces and allows the simulations of two phases of significantly different densities in the case of one component fluid. Both of these models have unphysical properties, e.g., the inconsistency between thermodynamic and kinetic pressure [11]. In the Shan and Chen model the surface tension is given by strength of the microscopic interaction and the shape of the density profile at the liquid-gas interface. Although it is possible to adjust these two independently, keeping the density profile constant and changing the surface tension requires the adjustment of two parameters. Furthermore the absolute value of surface tension is not known prior to evaluation of the density profile on the interface. A third LB model of immiscible fluids was proposed by Swift *et al.* [11] using a free-energy approach. Their model is constructed so that the pressure tensor is consistent with the tensor derived from the free-energy function of nonuniform fluids. This model leaves the interface width relatively wide. There also exists a class of LB models that are derived from kinetic equations [12]. These models can simulate two-phase miscible and immiscible fluid flow depending upon the choice of the inteparticle interactions. However in these models the magnitude of the surface tension is not known [12]. Collectively, these models have been applied to a multitude of multiphase flow problems, including the verification of Laplace law and capillary wave dispersion [9,13,14], spinoidal decomposition [15,16], studies of the Rayleigh-Taylor instability [7], free surface flow [17], flows in porous media [18–20], contact line motion [21], and diffusivity [12].

All of the above models have their positive and negative properties and the use of one instead of the other is a question of taste and of the application of interest. Here we study a modified version of the color-gradient method for three reasons. First the interfacial width is small and hence the position of the interface can be known accurately; second, the value of the surface tension is easy to calculate and adjust; and third, it is straightforward to control the contact angle and the wetting tendency of the solid phase. All of these properties are advantages when studying complex interface motion in confined and/or complex geometries.

We focus our attention on a problem of lattice pinning. We first discuss the origin of the pinning and show how it can be removed by changing the color redistribution scheme. We then go on to analyze the diffusive properties of the new color redistribution and explain why the width of the interfacial region in this type of models is set by a single parameter β that appears in the previous work of d'Ortona *et al.* [22]. We propose that β plays the role of an inverse length scale and show that the fully developed interfacial curve can be accurately predicted. We also show how spontaneous phase separation takes place in models of this type.

The remainder of this paper is organized as follows. In Sec. II the LB color gradient method is reviewed. In Sec. III we describe the lattice pinning problem. Section IV contains our solution to the lattice pinning problem. In Sec. V we discuss the interfacial properties of the improved method. Finally Sec. VI contains a description of spontaneous phase separation.

II. METHOD

The LB method [1–3,5] is constructed on a regular lattice face-centered hypercubic (FCHC) lattice. At each lattice point the populations $N_i^\sigma(\mathbf{x},t)$ are known. The subscript i denotes the lattice direction $\mathbf{c}_i$ connecting two neighboring lattice sites, the superscript σ denotes the particle type (red or blue particles in the color gradient method), $\mathbf{x}$ is the position in the lattice, and t is the simulation time step. These give the density, the velocity and the pressure/stress of the fluid at a given point.

Each simulation time step consists of the following steps.

(1) *Propagation*: Particle populations hop to neighboring sites, $N_i^\sigma(\mathbf{x}+\mathbf{c}_i,t)=N_i^{\sigma\prime}(\mathbf{x},t-1)$.

(2) Calculation of pseudoequilibrium populations $N_i^{\sigma(\mathrm{eq})}$,

$$N_i^{\sigma(\mathrm{eq})}(N^\sigma,\mathbf{u}) = N^\sigma\left(\frac{1-d_0}{b}+\frac{D}{c^2 b}\mathbf{c}_i\cdot\mathbf{u}+\frac{D(D+2)}{2c^4 b}\mathbf{c}_i\mathbf{c}_i{:}\mathbf{u}\mathbf{u}-\frac{D}{2bc^2}\mathbf{u}\cdot\mathbf{u}\right), \tag{1}$$

$$N_0^{\sigma(\mathrm{eq})}(d_0,\mathbf{u}) = N^\sigma\left(d_0-\frac{1}{c^2}\mathbf{u}\cdot\mathbf{u}\right). \tag{2}$$

These quantities have the following interpretations: N^σ is the number of particles of type σ, and $\mathbf{u}$ is the fluid velocity. $0<d_0<1$ is the proportion of the rest particles, which determines the compressibility of the fluid. We use $d_0=1/3$. b is the number of lattice directions, which for the FCHC lattice has the value $b=24$. c^2 is the length of the vectors $\mathbf{c}_i$ squared, which for the FCHC is $c^2=2$, and D is the dimension of the lattice. (For the FCHC lattice is $D=4$.) The pseudoequilibrium populations are chosen in such a way that in the long-wavelength limit the Navier–Stokes equations with an ideal gas equation of state are obtained [5,6,10].

(3) *Collision*: The populations N_i^σ relax towards the pseudoequilibrium distributions,

$$N_i^{\sigma\prime}(\mathbf{x},t) = (1+\lambda)N_i^\sigma(\mathbf{x},t)-\lambda N_i^{\sigma(\mathrm{eq})}(\mathbf{x},t). \tag{3}$$

Here λ is a relaxation parameter which acts as an inverse relaxation time. It also sets the value of kinematic viscosity, i.e., $\nu=-[c^2/\lambda(D+2)]-[c^2/2(D+2)]$ [5,6,10]. These collision and relaxation rules lead to the following macroscopic mass and momentum equations [5]:

$$\partial_t\rho+\boldsymbol{\nabla}\cdot\mathbf{v}=0, \tag{4}$$

$$\partial_t\mathbf{v}+\mathbf{v}\cdot\boldsymbol{\nabla}\mathbf{v}=-\boldsymbol{\nabla}p+\nu\nabla^2\mathbf{v}, \tag{5}$$

where $\rho=\Sigma_{i,\sigma}N_i^\sigma$, $p=\frac{1}{3}\rho$, and $\mathbf{v}=\rho\mathbf{u}$.

(4) *External forces*: Addition of, e.g., gravity or a pressure gradient.

(5) Two-phase step, which is discussed further below.

In the simplest case two immiscible fluids are identical except they have different "color," red and blue. These two fluids are immiscible. The surface tension is introduced by creating an anisotropic pressure field. Particles are redistributed in such a fashion that there are more particles moving perpendicular to an interface than parallel to it. Consequently blue particles move preferentially towards blue particles and red particles towards red particles, inducing spontaneuos phase separation. The two-phase step in the color gradient method can roughly be divided into the following substeps.

(1) Calculation of the color gradient: For brevity we denote N^{red} with R and N^{blue} with B. We use the notation R_i and B_i for the numbers of red and blue particles traveling to lattice direction $\mathbf{c}_i$, respectively. We also set $N_i=R_i+B_i$. The color gradient is given by

$$\mathbf{f}(\mathbf{x},t)=\sum_i \mathbf{c}_i\sum_j\left[R_j(\mathbf{x}+\mathbf{c}_i,t)-B_j(\mathbf{x}+\mathbf{c}_i,t)\right]. \tag{6}$$

(2) Perturbation of the populations,

$$N_i'(\mathbf{x},t)=N_i(\mathbf{x},t)+A|\mathbf{f}(\mathbf{x},t)|\left[\frac{(\mathbf{c}_i\cdot\mathbf{f})^2}{\mathbf{f}\cdot\mathbf{f}}-\frac{1}{2}\right]. \tag{7}$$

The parameter A is linearly proportional to the magnitude of surface tension such that [5,9]

$$\sigma=\frac{-192\rho A}{\lambda}. \tag{8}$$

(3) Redistribution of color: Color but not mass is redistributed to minimize the diffusion of color across the interface [9]. The 18 directions $\mathbf{c_i}$ are ordered in descending order starting from the one closest to the color gradient. The directions closest to the color gradient are occupied by red particles and the rest with blue particles conserving the mass of each particle type. This step is considerably simplified and improved in this paper.

III. LATTICE PINNING

The color gradient method has a potentially serious drawback, lattice pinning. Consider the following situation: a lattice site is on or near an interface of blue and red fluid. Now suppose the fluids have a constant flow velocity everywhere on the lattice, but that this velocity is not high enough to move significant populations of red particles from one site to another. In this situation the interface cannot move and is pinned to the lattice.

In Fig. 1 we show how the velocity of a small red bubble depends on its size. We plot the average velocity of the red particles as a function of the effective radius of the bubble. This is given by $R=\sqrt{M/\rho\pi}$, where M is the mass of the bubble and ρ is the density of the fluid. As we see bubbles as large as seven full lattice sites ($R=1.49$) are completely pinned. Some of the smaller bubbles were not pinned, and we suspect this to be a result of the symmetric configurations available for the bubble at these sizes. This seems to depend on the initial conditions however, and any bubble smaller than $R<1.13$ is always pinned, any bubble between sizes $1.13<R<1.49$ is likely to be pinned, and any bubble between sizes 1.49 and 1.59 can become pinned.

What causes this lattice pinning? The clearest case of this phenomenon can be seen in very small bubbles of red fluid immersed in a blue sea. Figures 2 and 3 demonstrate one case. Although we show the small bubble case as a demonstration the effect persists on larger scales.

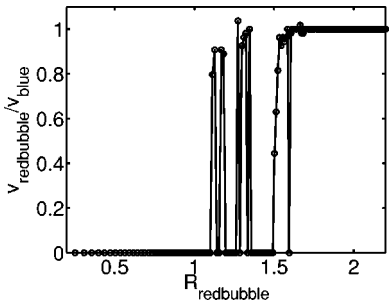

FIG. 1. We plot the average velocity of the red bubble as a function of the bubble size. $R_{\text{red bubble}}$ is the effective radius of the bubble, $v_{\text{red bubble}}$ is the average velocity of the bubble, averaged over 10 000 time steps, and v_{blue} is the velocity of the surrounding blue fluid.

For our purposes there are two specific cases where this effect is significant. In the first case, small bubbles (i.e., bubbles concentrated around a single lattice point) will not move unless they are forced very hard. This problem is significant when studying the separation and flow of an initally mixed state. The second case concerns nonwetting and wetting fluid that becomes stuck near walls, and leads to a history-dependent contact angle. In this paper we specifically address the first case; the latter will be discussed in a subsequent study [23].

In Fig. 3 we further study the lattice pinning presented in Fig. 2. Figure 3(a) gives the direction of the color gradient at each site. The directions closest to the color gradient are numbered. These directions are occupied by red particles, the last one being partially occupied by red and by blue. Figure 3(b) shows a graphical presentation of the concentration of red color at each site and of the excess flows from one site to the other. One can see that most of the red fluid is going around in a figure-eight shaped curve. What makes this possible? In the middle-left site the last direction to send red particles is the top-right direction and in the middle-right site the last direction to send red particles is the top-left direction. All these particles return to the middle-right and middle-left sites because the first direction to send particles on both top-left and top-right sites is the downwards direction.

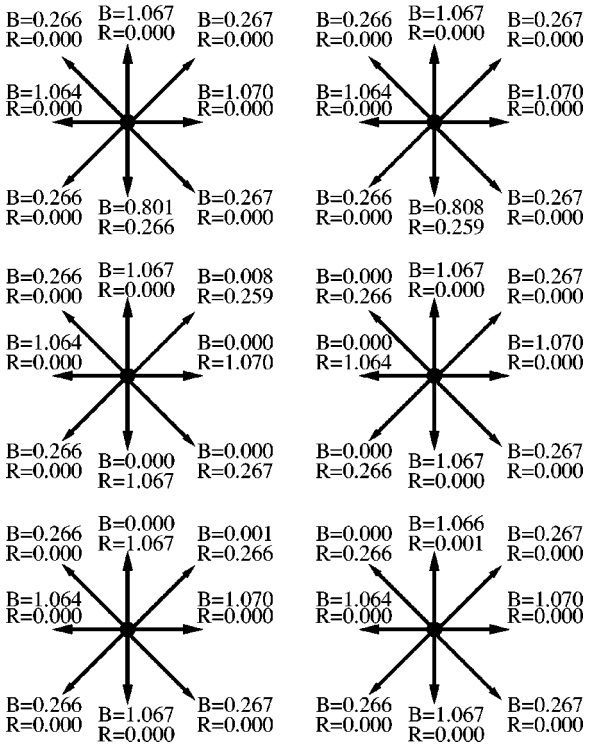

FIG. 2. Lattice pinning in action. The velocity at each lattice site is $N\mathbf{u}=\Sigma N_i\mathbf{c}_i=9.393\times10^{-3}\hat{\mathbf{x}}$. The red particles go around in small loops and at each site the number of red particles is conserved. While we have a nonzero flow velocity the red particles do not move, and are thus *pinned* to the lattice.

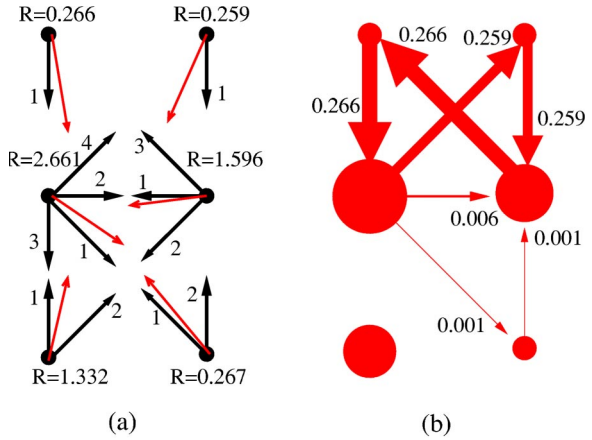

FIG. 3. (Color online) (a) The total red population at each site, and the directions of color gradients arising from this distribution. The directions closest to the color gradient are shown numbered, starting from the direction closest to the gradient. These directions send red particles, the last one sending a fraction of red and blue particles. The remaining directions send blue particles. (b) We show schematically the red populations at each site, and the amount of red particles moving through each link at each simulation time step. We have cancelled out equal and opposite currents hence showing only the excess flow of the red particles.

To understand this problem we make three important observations. First, we note that the red particle distribution is not symmetric with respect to the color gradient. Second, we notice that the lattice pinning does not necessarily have anything to do with the spurious currents that are present near a two-fluid interface [5]. In the example we are showing there are no spurious currents in $N_i=R_i+B_i$ (i.e., the red+blue fluid combination), nor are there any interfacial anisotropic pressure gradients, because A, the parameter controlling the surface tension, has been set to zero. The only reason that the red particles are pinned is because of the color redistribution. Because the directions close to the color gradient are filled with red particles in order of proximity, the red particles are allowed to wander around in circles. Our third observation is that there is a limit to lattice pinning. If the fluid velocity is high enough or if the bubble is large enough this kind of trapping phenomena cannot take place. It is essentially one partially filled direction that allows for the collective flow from left to right to be leaked back to the left. If the amount of the collective flow exceeds the "leak-back capacity" the

red fluid will move. The largest leak-back capacities are typically found in cases where there are sharp edges or cusps, like the small bubbles.

IV. IMPROVED METHOD

The crucial part of this solution is to allow the red and the blue fluids to moderately mix and to keep the color distribution symmetric with respect to the color gradient. The reason for lattice pinning is that at the sites where it happens all of the particles of one kind are sent to one direction and hence they cannot move from one site to another. An obvious way to fix this problem is to send only a fraction of particles of one color to these directions. This will also allow the interface to move slowly and without pinning. A solution to this problem has been proposed in a different context by d'Ortona *et al.* [22] and Tölke *et al.* [24]. The method of d'Ortona *et al.* sends a fraction of particles that is proportional to the inner product of the color gradient and the lattice direction in question. We changed the distributions of d'Ortona *et al.* slightly in order to make certain that no negative populations of either type of particles will occur. We use the following redistribution:

$$R_i = \frac{R}{R+B}N_i' + \beta\frac{RB}{(R+B)^2}N_i^{(\mathrm{eq})}(N,0)\cos\varphi, \tag{9}$$

$$B_i = \frac{B}{R+B}N_i' - \beta\frac{RB}{(R+B)^2}N_i^{(\mathrm{eq})}(N,0)\cos\varphi, \tag{10}$$

Here R_i and B_i are the numbers of red and blue particles going to direction $\mathbf{c}_i$, R and B are the total numbers of red and blue particles at a given site, N_i' is defined by Eq. (7), $N_i^{(\mathrm{eq})}(N,0)$ is the zero-velocity equilibrium distribution, β is a parameter giving the tendency of the two fluids to separate, and φ is the angle between the color gradient $\mathbf{f}$ and the direction $\mathbf{c}_i$. Without the last term in the equations, red and blue particles would be distributed according to their numbers and there would be no tendency for the fluids to separate. β can take any value between 0 and 1. As β increases the interface is less diffuse, i.e., β sets the surface width. If $\beta>1$ there can be negative populations of particles, but if these are kept small the stability is maintained.

We test the model in the case of small bubbles as in Sec. III. We initialize the lattice with fluid that has a constant flow velocity $\mathbf{u}=5.4\times10^{-3}\hat{\mathbf{x}}$. Any velocity can be chosen for qualitatively similar behavior. We use a two-dimensional system of size 30×30 with fluid density $N=10$, and initialize a small red bubble in the center of this space. The size of this bubble is adjustable. In Fig. 4 we plot the average velocity of the red bubble averaged over 10 000 time steps after the steady state has been reached as a function of bubble mass, for the improved method when $\beta=1.0$, 0.9, 0.8. We plot the average velocity of the red bubble averaged over 10 000 time steps after the steady state has been reached.

For $\beta=1.0$ only bubbles smaller than size 18 are completely pinned. As the bubble size increases the velocity approaches the surrounding fluid velocity. As the value of β decreases the pinning threshold also decreases. Small unpinned bubbles tent to move in bursts, i.e., they remain essentially pinned for a while, then jump to the next lattice site and so on. We suspect that, because of the ability for the two fluids to mix, the largest leak-back-capacity is eventually filled and the bubble is allowed to move to the next site.

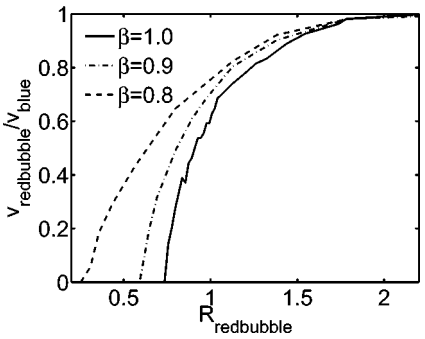

FIG. 4. Comparison of the old method to the improved method. The units are the same as in Fig. 1. $R_{\text{red bubble}}$ is the effective radius of the bubble, $v_{\text{red bubble}}$ is the average velocity of the bubble, averaged over 10 000 time steps, and v_{blue} is the velocity of the surrounding blue fluid. For $\beta=1.0$ only bubbles smaller than size $R<0.75$ are completely pinned, and for smaller β this size is even reduced. In the case of the old method, bubbles as large as size $R=1.59$ could be pinned and all bubbles smaller than $R<1.16$ are always pinned.

Comparing Fig. 4 to Fig. 1, we see that the improved method clearly reduces the problem of lattice pinning. We suspect that the ability to form symmetrical bubbles at smaller sizes and the slightly larger bubble radius are responsible for this effect. The lattice pinning is not completely removed when $\beta=1.0$, but its effects are reduced. Other advantages of the new method include the ability to remove history dependent contact angles [23] and the relative smoothness of the interfaces. Significantly, the improved method is much easier to implement than the old method.

V. DIFFUSIVE PROPERTIES

In this section we study the diffusive properties of the model, more specifically how spontaneous phase separation takes place. We first consider an extremely simplified case of a one-dimensional diffusive D1Q2 model [25], with zero velocity everywhere. In this model there are two velocities $\mathbf{c}_1=\hat{\mathbf{x}}$ and $\mathbf{c}_2=-\hat{\mathbf{x}}$. The equilibrium distributions are $N_i^{(\mathrm{eq})}(\mathbf{x},t)=\rho(\mathbf{x},t)/2$. If the system starts from the case of zero velocity everywhere and constant density ρ then $N_i(\mathbf{x},t)=\rho/2$ for all $\mathbf{x}$ and t. Then Eqs. (9) and (10) can be written as

$$R_i(\mathbf{x},t) = R(\mathbf{x},t)/2 + \mathrm{sgn}(\mathbf{f})(-1)^{i-1}\beta\phi(\mathbf{x},t)[1-\phi(\mathbf{x},t)],$$

$$i=1,2, \tag{11}$$

$$B_i(\mathbf{x},t) = B(\mathbf{x},t)/2 - \mathrm{sgn}(\mathbf{f})(-1)^{i-1}\beta\phi(\mathbf{x},t)[1-\phi(\mathbf{x},t)],$$

$$i=1,2, \tag{12}$$

where ϕ is the fraction of red particles, i.e., $\phi=R/\rho$, $\mathrm{sgn}(\mathbf{f})=1$ if $\mathbf{f}$ points to the x direction, $\mathrm{sgn}(\mathbf{f})=-1$ if $\mathbf{f}$ points to $-x$ direction, and $\mathrm{sgn}(\mathbf{f})=0$ if $\mathbf{f}=0$.

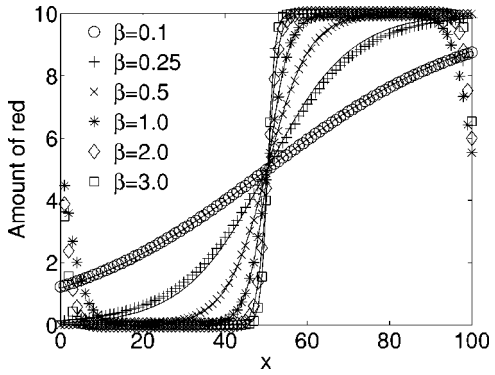

FIG. 5. One-dimensional diffusive multiphase LB model. We plot the fully developed stable interfacial curves as a function of β. For $\beta \geqslant 1.0$ the system size is 100 lattice sites; for $\beta \leqslant 0.5$ we use a larger system size of 500 lattice sites in order to obtain fully developed interfacial curves. Periodic boundary conditions are used. The smooth curves show the theoretical prediction of Eq. (17).

It is easy to see that if there is no color gradient, i.e., $\mathbf{f} \equiv 0$, then the distributions R_i and B_i do not change. This means that $R(\mathbf{x},t) \equiv R$ and $B(\mathbf{x},t) \equiv B$ is an equilibrium distribution. However this distribution is unstable. Even the smallest change from it will lead to spontaneous phase separation. It is also relatively straightforward to see that any linear ramp, i.e., $R(\mathbf{x},t) = a + b(x - x_0)$ and $B(\mathbf{x},t) = N - R(\mathbf{x},t)$ is an equilibrium distribution. This is because at each node within the ramp the number of blue and red particles is conserved. This distribution is even stable to small deviations, i.e., deviations that do not change the direction of the color gradient at any of the nodes. However in the case of a linear ramp there is a net flow of red particles towards the excess of red particles and a net flow of blue particles towards the excess of blue particles. Hence this distribution cannot stay stable in a closed system with no sources or sinks of blue and red particles. To find the stable equilibrium distribution of red and blue particles in the case of a closed system, we initialize a lattice of 100 sites with a linear ramp $R(x,t) = 5.0 + 2.0(x - 50)$ and $B(x,t) = 10.0 - R(x,t)$ and used periodic boundary conditions. The results as a function of β are shown in Fig. 5.

The resulting fully developed interfacial curves may be quantitatively predicted. Because there are no currents of either blue or red particles in steady state, at each site the number of red particles leaving the site to the left-hand side must equal the number of red particles arriving from the left-hand side. Consider a situation where the color gradient points towards the right-hand side. Let the amount of red particles on the site on the left-hand side be R and on the site on the right-hand side be $R + \omega$. Then

$$R/2 + \beta\phi(1 - \phi) = (R + \omega)/2 - \beta\phi(1 - \phi),$$

$$\omega = 4\beta\phi(1 - \phi). \tag{13}$$

The first derivative of ϕ can be approximated as

$$\frac{d\phi}{dx} = \frac{R + \omega}{N} - \frac{R}{N} = \frac{\omega}{N}. \tag{14}$$

If these two equations are combined one finds

$$\frac{d\phi}{dx} = \frac{4\beta}{N}\phi(1 - \phi). \tag{15}$$

This equation for the shape of the fully developed interfacial curve is the same for all models using the improved color gradient method [i.e., Eqs. (9) and (10)]; only the prefactor $K(\beta)$ changes. The solution to Eq. (15) gives

$$\phi(x) = \frac{Ce^{K(\beta)x}}{1 + Ce^{K(\beta)x}}. \tag{16}$$

If one further knows the midpoint of the interface, i.e., where $\phi(x = x_0) = 0.5$, the full form of the equation is known,

$$\phi = \frac{e^{K(\beta)(x - x_0)}}{1 + e^{K(\beta)(x - x_0)}}. \tag{17}$$

In Fig. 5 we plot these curves versus the measured interfacial curves and can see an excellent agreement. We also see why β sets the length scale. On large scales $[x - x_0 \gg 1/K(\beta)]$ one always sees red particles separated from blue particles. At the interfacial regions the red and the blue particles mix. The width of the interfacial regions is given by $K^{-1}(\beta)$. The interfacial length scale is therefore inversely proportional to β. For $\beta = 1$ and the one-dimensional model ($N = 10$, $\phi = 0.5$) we obtain a length scale of 10, which is consistent with Fig. 5.

We next investigate the one-dimensional projection of the full four-dimensional FCHC LB model presented in the first section. We set $A = 0$, but we also show, just as in Ref. [22], that this parameter has only a weak effect on the interfacial curve. The amount of particles traveling from right to left (or left to right) is $\frac{1}{18}N + 4\frac{1}{36}N = \frac{1}{6}N$. The amount of total change caused by the color gradient is $\left[\frac{1}{18} + \frac{4}{36}(1/\sqrt{2})\right]/\beta N\phi(1 - \phi) = [(1 + \sqrt{2})/18]\beta N\phi(1 - \phi)$. If we combine these we find

$$\frac{R}{6} + \frac{1 + \sqrt{2}}{18}\beta N\phi(1 - \phi) = \frac{R + \omega}{6} - \frac{1 + \sqrt{2}}{18}\beta N\phi(1 - \phi) \tag{18}$$

and therefore

$$\frac{d\phi}{dx} = \frac{2}{3}(1 + \sqrt{2})\beta\phi(1 - \phi). \tag{19}$$

therefore $K(\beta) = \frac{2}{3}(1 + \sqrt{2})\beta$.

In Fig. 6 we show the fully developed interfacial curve for the one-dimensional projection of the full three-dimensional LB model with the improved color gradient scheme. The interfacial curves for different β are collapsed onto a single curve by rescaling the x axis with β. The curve going through the data points is given by Eq. (16) with $K(\beta)$ given by (19).

In Fig. 7 we show how the interfacial curve changes as a function of A. Here we choose $\beta = 1$. We see little or no change as expected.

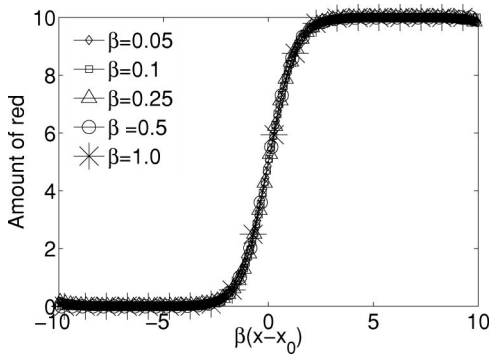

FIG. 6. The fully developed interfacial curve for the one-dimensional projection of the three-dimensional LB method. The curves with different β are collapsed into a single curve by rescaling the x axis.

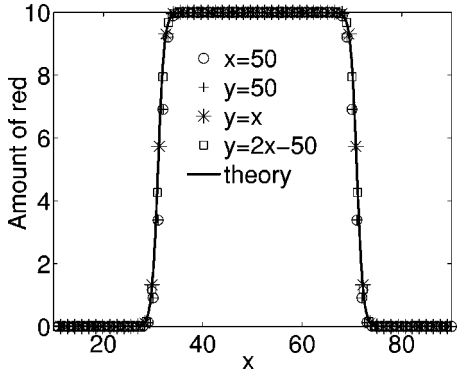

FIG. 8. The interfacial curve for two-dimensional bubble. We plot the amount of the red fluid as a function of position. We have bisected the bubble in four different directions. The solid line is the theoretical curve given by Eqs. (17) and (19).

We next study the method in a two-dimensional system. We initialized a red bubble of radius 20 in a system of size 100×100, i.e., we filled sites for which $(x-50)^2+(y-50)^2<20^2$ with red fluid and the rest of the sites with blue fluid at rest. After 100 timesteps a fully developed interfacial curve is reached. The interface is fully symmetric and the curve has the same predicted shape in all directions. The interfacial curve for this bubble in the case of $\beta=1.0$ is shown in Fig. 8. We also initialized a red bubble of radius 20 in a fully three-dimensional system of size $100\times100\times100$ obtaining a fully developed interfacial curve in all directions.

VI. SPONTANEOUS PHASE SEPARATION

To further understand the onset of the spontaneous phase separation, we study in this section a case where small numerical errors lead to a rapid phase separation. We tested the model in a three-dimensional system with periodic boundary conditions and system size of $30\times3\times3$ lattice sites, with a linear ramp in x direction. Figure 9 shows the results schematically, and Fig. 10 shows the phase separation explicitly. We started the system as in the case of one-dimensional case with a linear ramp, i.e., $N=10\,R(\mathbf{x},t=0)=5.0+2.0(x-15)$ and $B=N-R$.

In the early stages the system behaves exactly as the one-dimensional system but at one point due to round-off errors one of the sites becomes slightly less red. This small error causes the color gradient close to it to point away as seen in Fig. 9 and slowly but certainly this small deviation grows larger. When it becomes large enough it spreads to the neighboring sites and at one point there is a reversal of the direction of the color gradient at one of the sites (from positive x-direction to negative x-direction). This leads to a nucleation of a quasi-one-dimensional red bubble. At the points of the color gradient reversal both the left-hand side and the right-hand side try to develop towards the fully developed interfacial curve, but because there is not enough space and the system is effectively one-dimensional, the color is trapped into small red and blue islands. The change in the interfacial curve is largest at these gradient reversal sites. If there would be no reversals the system would always evolve towards the fully developed interfacial curve.

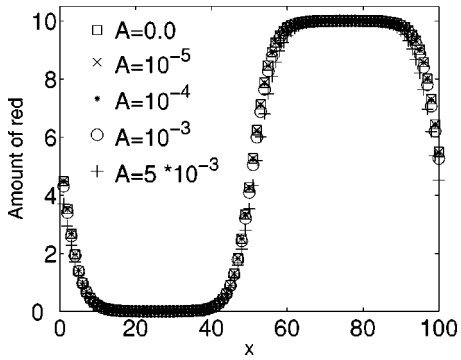

FIG. 7. Surface tension included. As the A parameter changes the surface width remains the same. We use $\beta=1$.

Once these red and blue islands have formed the relative differences between the red and blue content within the island continues to decrease, i.e., within the island (in the y and z directions) the behavior of the system is diffuse. There are two reasons for this: first, the color gradient is largest in the x direction; and second, there is no space for the interfa-

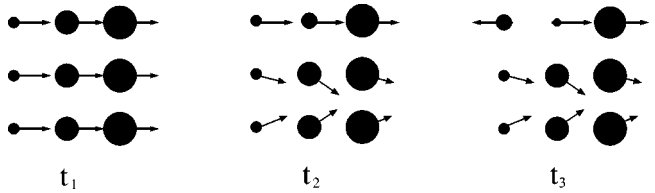

FIG. 9. Early stages of spontaneous phase separation in quasi-one-dimensional system, at times $t_1<t_2<t_3$. We show the relative amounts of red particles as the sizes of the circles and the color gradients with an arrow. The system has periodic boundary conditions in (t_1) direction. In the beginning $y$all the color gradients are pointing straight to the right-hand side. At some point (t_2)one of the sites gets a little less red particles than it's supposed to and this turns the color gradients away from that row. The column that contained the original site is affected the strongest. This leads at one point to a reversal of the direction of the color gradient (t_3). Eventually this induces the reversal in the whole column and spontaneous phase separation takes place.

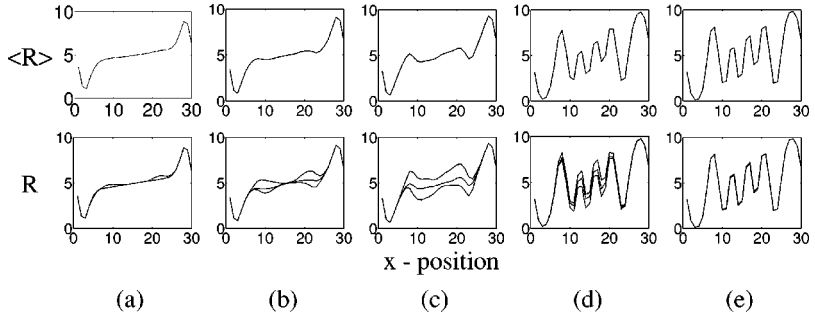

FIG. 10. Steps of spontaneous phase separation in quasi-one-dimensional system. The system size is $30\times3\times3$. On the bottom we plot the amount of red as a function of x for all three values of $y=1$, 2, 3. On the top we plot the amount of these combined as a function of x. The progress in time is shown from left-hand to right-hand sides. These distributions are taken at times $t=10$, $t=12$, $t=14$, $t=25$, and $t=35$. At first two of the rows ($y=1$) gets separated from the third (a). Then there is a color gradient reversal inside a row (b). This eventually leads to color gradient reversals for the x columns (c). Finally there is spontaneuous phase separation (d) and (e).

cial curve to develop in the y and z directions. The color gradient is largest in the x direction because that is its original direction. Even after the color gradient obtains y and z components due to the numerical errors this direction remains dominant. This is because the increase in the color gradient in the y and z directions is limited by the system size. The antidiffuse behavior (i.e., separation of phases) takes place in the direction of the color gradient. In the directions perpendicular to the color gradient there is no antidiffuse tendency and the two phases mix. The blue and red particles are therefore mixed in these islands.

We have shown that if there is a color gradient present in the system it tries to evolve towards a fully developed interfacial curve. This development separates the two fluids. The development starts from the places with color gradient inversions, i.e., places where $|\nabla^2\phi|$ attains its maxima, and propagates outwards. This behavior is similar to the early stages of spinoidal decomposition, see, e.g., Ref. [26]. In fact it should be possible to measure the antidiffusivity as a function of β by measuring how the interfacial curve changes. If there is no space for one colored fluid to go this process stops. In one dimension with zero velocity no gradient inversion is reversible and all fluid becomes stuck into these small islands. In two and higher dimensions the process continues as long as the fluid has a chance to connect with other fluid of the same kind. The interfaces of small bubbles may not be fully developed but larger ones are. When one adds surface tension into the equation the system starts trying to minimize the surface area between red and blue fluids and the separation continues. The separation always happens regardless of β. β merely sets the length scale of the interface.

VII. CONCLUSIONS

We have reported and quantified a problem of lattice pinning associated with the LB color gradient method. These problems can be fixed by changing the recoloring step and allowing wider interfaces. This improved recoloring step is much easier to implement than the old one. With the improved method the distribution of red and blue particles is symmetric around the color gradient. We have studied interfacial and phase separation properties of the improved method and have shown that the method significantly diminishes the problem of lattice pinning. The analytical expression for the shape of the interfacial curve is found, and the parameter β is shown to act as a measure for the inverse interfacial width.

ACKNOWLEDGMENT

This work was supported by the Office of Science (BER), U.S. Department of Energy, Grant No. DE-FG07-02ER63490.

[1] G. McNamara and G. Zanetti, Phys. Rev. Lett. **61**, 2332 (1988).
[2] F. J. Higuera and J. Jimenez, Europhys. Lett. **9**, 663 (1989).
[3] Y. Qian, D. d'Humières, and P. Lallemand, Europhys. Lett. **17**, 479 (1992).
[4] D. H. Rothman and S. Zaleski, Rev. Mod. Phys. **66**, 1417 (1994).
[5] D. Rothman and S. Zaleski, *Lattice Gas Cellular Automata* (Cambridge University Press, Cambridge, 1997).
[6] S. Chen and G. D. Doolen, Annu. Rev. Fluid Mech. **30**, 329 (1998).
[7] X. He, S. Chen, and R. Zhang, J. Comput. Phys. **152**, 642 (1999).
[8] L. S. Luo, Phys. Rev. E **62** 4982 (2000).
[9] A. K. Gunstensen, D. H. Rothman, S. Zaleski, and G. Zanetti, Phys. Rev. A **43**, 4320 (1991); A. K. Gunstensen and D. H. Rothman, Europhys. Lett. **18**, 157 (1992).
[10] X. Shan and H. Chen, Phys. Rev. E **47**, 1815 (1992).
[11] M. R. Swift, W. R. Osborn, and J. M. Yeomans, Phys. Rev. Lett. **75**, 830 (1995); M. R. Swift, E. Orlandini, W. R. Osborn, and J. M. Yeomans, Phys. Rev. E **54**, 5041 (1996).
[12] Z. Guo and T. S. Zhao, Phys. Rev. E **71**, 026701 (2005).

[13] D. Grunau, S. Chen, and K. Eggert, Phys. Fluids A **5**, 2557 (1993).
[14] X. Shan and H. Chen, Phys. Rev. E **49**, 2941 (1994).
[15] F. J. Alexander, S. Chen, and D. W. Grunau, Phys. Rev. B **48**, 634 (1993).
[16] W. R. Osborn, E. Orlandini, M. R. Swift, J. M. Yeomans, and J. R. Banavar, Phys. Rev. Lett. **75**, 4031 (1995).
[17] I. Ginzburg and K. Steiner, J. Comput. Phys. **185**, 61 (2003).
[18] A. Gunstensen and D. Rothman, J. Geophys. Res., [Planets] **98**, 6431 (1993).
[19] Q. Kang, D. Zhang, S. Chen, and X. He, Phys. Rev. E **65**, 036318 (2002).
[20] C. Manwart, U. Aaltosalmi, A. Koponen, R. Hilfer, and J. Timonen, Phys. Rev. E **66**, 016702 (2002).
[21] A. J. Briant and J. M. Yeomans, Phys. Rev. E **69**, 031603 (2004).
[22] U. D'Ortona, D. Salin, M. Cieplak, R. Rybka, and J. Banavar, Phys. Rev. E **51**, 3718 (1995).
[23] M. Latva-Kokko and D. Rothman (unpublished).
[24] J. Tölke, M. Krafczyk, M. Schultz, and E. Rank, Philos. Trans. R. Soc. London, Ser. A **360**, 535 (2002).
[25] Y. H. Qian and S. Orszag, J. Stat. Phys. **81**, 237 (1995).
[26] J. Gunton, M. S. Miguel, and P. Sahni, in *Phase Transitions and Critical Phenomena*, edited by C. Domb and J. L. Lebowitz (Academic, New York, 1983), Vol. 8, pp. 269–482.